Molecular Therapy
Original Article

Perivascular Stem Cell-Derived Cyclophilin A Improves Uterine Environment with Asherman's Syndrome via HIF1α-Dependent Angiogenesis

Mira Park,[1,8] Seok-Ho Hong,[2,8] So Hee Park,[1] Yeon Sun Kim,[1] Seung Chel Yang,[1] Hye-Ryun Kim,[1] Songmi Noh,[3] Sunghun Na,[4] Hyung Keun Lee,[5] Hyunjung J. Lim,[6] Sang Woo Lyu,[7] and Haengseok Song[1]

[1]Department of Biomedical Science, CHA University, Seongnam 13488, Korea; [2]Department of Internal Medicine, Kangwon National University, Chuncheon, Kangwon 24341, Korea; [3]Department of Pathology, CHA Gangnam Medical Center, CHA University, Seoul 06135, Korea; [4]Department of Obstetrics and Gynecology, School of Medicine Kangwon National University, Chuncheon, Kangwon 24341, Korea; [5]Institute of Vision Research, Department of Ophthalmology, Yonsei University College of Medicine, Seoul 06273, Korea; [6]Department of Veterinary Medicine, Konkuk University, Seoul 05029, Korea; [7]Fertility Center of CHA Gangnam Medical Center, CHA University, Seoul 06135, Korea

Asherman's syndrome (AS) is characterized by intrauterine adhesions or fibrosis resulting from scarring inside the endometrium. AS is associated with infertility, recurrent miscarriage, and placental abnormalities. Although mesenchymal stem cells show therapeutic promise for the treatment of AS, the molecular mechanisms underlying its pathophysiology remain unclear. We ascertained that mice with AS, like human patients with AS, suffer from extensive fibrosis, oligo/amenorrhea, and infertility. Human perivascular stem cells (hPVSCs) from umbilical cords repaired uterine damage in mice with AS, regardless of their delivery routes. In mice with AS, embryo implantation is aberrantly deferred, which leads to intrauterine growth restriction followed by no delivery at term. hPVSC administration significantly improved implantation defects and subsequent poor pregnancy outcomes via hypoxia inducible factor 1α (HIF1α)-dependent angiogenesis in a dose-dependent manner. Pharmacologic inhibition of HIF1α activity hindered hPVSC actions on pregnancy outcomes, whereas stabilization of HIF1α activity facilitated such actions. Furthermore, therapeutic effects of hPVSCs were not observed in uterine-specific HIF1α-knockout mice with AS. Secretome analyses of hPVSCs identified cyclophilin-A as the major paracrine factor for hPVSC therapy via HIF1α-dependent angiogenesis. Collectively, we demonstrate that hPVSCs-derived cyclophilin-A facilitates HIF1α-dependent angiogenesis to ameliorate compromised uterine environments in mice with AS, representing the major pathophysiologic features of humans with AS.

INTRODUCTION

The human endometrium undergoes extensive remodeling that is unparalleled in any other adult organ.[1] Asherman's syndrome (AS) is characterized by intrauterine adhesions (IUAs) and/or fibrosis caused by the destruction of the basal layer of the endometrium,[2,3] where endometrial stem/progenitor cells are believed to reside.[4] Thus, severe damage to this basal layer may destroy endometrial stem/progenitor cells and result in the loss of regeneration potential.[5] In fact, trauma to the endometrial basal layer can lead to the loss of a functional endometrium and result in menstrual disturbances, such as amenorrhea/oligomenorrhea.[6] AS is closely associated with infertility, recurrent miscarriage, and placental abnormalities.[7,8] The conventional treatment for AS is hysteroscopic adhesiolysis followed by estrogen therapy, which has been shown to significantly improve fertility outcomes.[7] Nonetheless, the treatment of severe cases is very difficult. Various modalities with conventional treatment have been applied including vasoactive measures and growth factor(s).[9] However, most of the treatments only achieve minor changes for endometrial regeneration and subsequent pregnancy outcomes.[9–11]

Autologous bone marrow-derived mesenchymal stem cells (BM-MSCs) are considered the gold standard of MSC therapies to treat various tissue injuries.[12] However, due to the limited availability of cells and/or reductions in growth and differentiation capacities with age,[13] there is a clear need for novel sources that have their own benefits and bypass the disadvantages of autologous BM-MSCs. In this aspect, perivascular stem cells derived from human umbilical cords (hUC-PVSCs) are an attractive alternative due to the ease and noninvasive method of harvesting large numbers of MSCs with a low risk of infection.[14] Recently, human PVSCs (hPVSCs) were reported to be a common ancestor of different types of MSCs,[15] have greater proliferation and differentiation potentials than BM-MSCs, and have low immunogenicity with good immunosuppressive properties.[16,17]

Received 2 March 2020; accepted 14 May 2020;
https://doi.org/10.1016/j.ymthe.2020.05.015.

[8]These authors contributed equally to this work.

Correspondence: Haengseok Song, Department of Biomedical Science, CHA University, Seongnam 13488, Korea.
E-mail: hssong@cha.ac.kr
Correspondence: Sang Woo Lyu, Fertility Center of CHA Gangnam Medical Center, CHA University, Seoul 06135, Korea.
E-mail: dung5038@cha.ac.kr

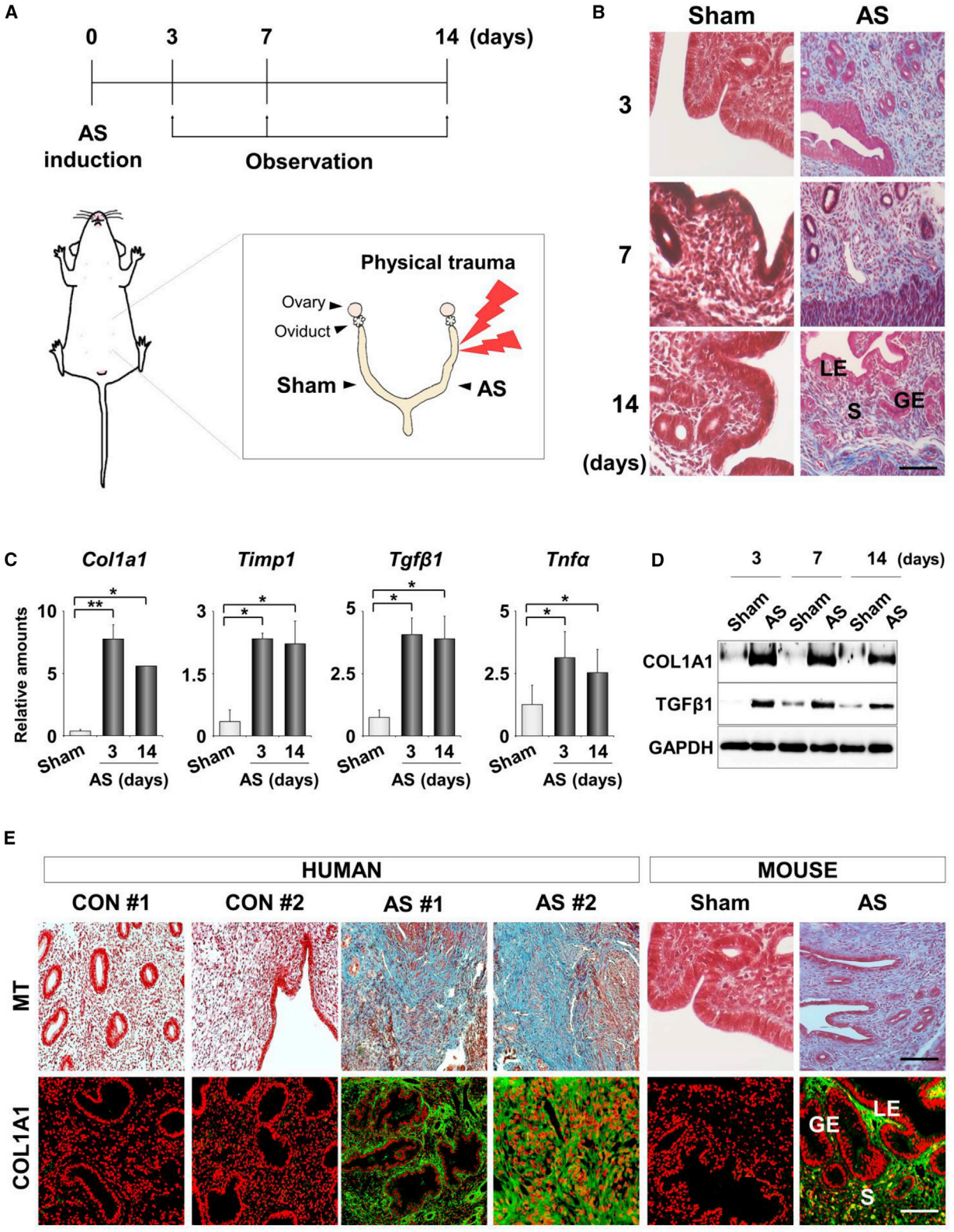

(legend on next page)

The application of hPVSCs from various sources facilitates effective regeneration of damaged tissues, including heart, skeletal muscle, bone, and lung.[18–20] Recently, human endometrial PVSCs were shown to contribute to functional uterine regeneration in rat models of partial uterine excision.[21] Although a few pilot studies have suggested that MSCs may facilitate regeneration of the damaged endometrium in humans and rodent models with AS,[22,23] underlying molecular mechanisms of beneficial effects of MSCs on the endometrium with AS still remain unclear. Here, we demonstrated that the endometrium with AS is functionally compromised so that embryo implantation is aberrantly delayed, which leads to intrauterine growth restriction (IUGR) and miscarriage. Using pharmacologic and genetic tools, we uncovered that hUC-PVSCs secrete paracrine factors, such as cyclophilin A (CYP-A), that improved compromised uterine environments via hypoxia inducible factor 1α (HIF1α)-dependent angiogenesis in mice with AS.

RESULTS

A Murine Model of AS Recapitulates Representative Histologic and Molecular Features of AS in Humans

A murine model of AS was experimentally induced by a physical insult to the uterine horns (Figure 1A). Histologic analyses of the damage in these mice showed severe fibrosis with morphologic disturbances in the uterine structures (Figure 1B). The gross histology of traumatized uteri appeared to recover 2 weeks after the trauma. However, the expression profiles of the molecular markers of fibrosis, such as *Col1a1*, *Timp1*, transforming growth factor β1 (*Tgfβ1*), and tumor necrosis factor alpha (*Tnfα*), demonstrated that the fibrosis-associated pathologic conditions were thoroughly maintained in uteri with AS at all days examined (Figures 1C and 1D). Fibrotic lesions, which appear blue by Masson's trichrome (MT) staining, and COL1A1 (collagen) accumulation, which were observed by immunofluorescence (IF) staining, were clearly evident in the endometrial tissues from patients with AS but not from healthy women (Figure 1E). These results suggest that the murine model of human AS used in this study recapitulates the representative features of AS in humans.

hPVSCs Facilitate Regeneration and Reduce Fibrosis in the Uteri of Mice with AS

We validated the fundamental features of hPVSCs as MSCs before we examined the therapeutic potential of hPVSCs. FACS flow cytometer analyses demonstrated that hPVSCs share general markers with other MSCs, including $CD31^-$, $CD34^-$, $CD45^-$, $CD44^+$, and $CD90^+$. In addition, hPVSCs have specific features, such as $CD146^+$ with a subpopulation of $SSEA\text{-}4^+$ (Figure S1A). hPVSCs successfully differentiated into multiple lineages, as demonstrated by the appearance of chondrogenic, adipogenic, and osteogenic properties (Figure S1B). To evaluate the therapeutic potential of hPVSCs, we administered these cells to one of two AS uterine horns via intrauterine (IU) delivery and then examined histologic and molecular markers of fibrosis (Figure 2A). IU delivery of hBM-MSCs was performed as a positive control for MSC therapies on AS uteri. MT staining and COL1A1 IF staining showed that hPVSCs dramatically reduced fibrotic lesions in damaged uteri. Furthermore, IF staining of KI-67, a cell proliferation marker, showed that hPVSCs promoted cell proliferation during regeneration in AS uterine horns. Similar to hBM-MSCs, single IU delivery of hPVSCs (1×10^6) significantly dampened the increased expression of fibrosis-associated factors in AS uteri at the mRNA (Figure 2B) and protein levels (Figure 2C).

hPVSCs Improve the Chronic Impairment of the Uterine Environment in Mice with AS

We established two protocols to evaluate the therapeutic function of hPVSCs on pregnancy outcomes in mice with AS; namely, a single IU delivery of 1×10^6 hPVSCs (group I, hPVSCs+) and a single IU delivery of 1×10^6 hPVSCs followed by three intraperitoneal (i.p.) deliveries (group II, hPVSCs+++). Then, the time to become pregnant, the delivery rate, and the litter size were examined in mice with AS (Figure 2D). As expected, sham controls took approximately 4 days to conceive. However, a greater than 6-fold longer time period was required for mice with AS to become pregnant ($p < 0.01$), suggesting an oligomenorrhea-like phenotype. Both transplantation protocols significantly reduced the time to conceive, although they did not reach the level of the sham controls (Figure 2E). With regard to delivery rate, none of the mice with AS (0/6) produced any pups, whereas all sham controls (4/4) and mice with AS that were administered hPVSCs delivered healthy pups (Figure 2F). Furthermore, the mean litter size was also significantly increased in mice with AS that were administered hPVSCs (+ and +++ had 2.5 ± 0.6 and 8.0 ± 2.8 pups, respectively) in a dose-dependent manner (Figure 2G).

Because chronic and recurrent IUAs with fibrosis could be the main causes of infertility in patients with AS,[22,24] it was imperative to examine whether these pathophysiological features persistently interfered with uterine functions in our AS model. Thus, second pregnancy outcomes of mice with AS were examined (Figure S2A). Although the time to conceive the second pregnancy was shorter than the time to conceive the first pregnancy in mice with AS, it was still significantly longer (~3.5 times) than the sham controls (Figure S2B). Accordingly, 66% (4/6) of mice with AS delivered pups (Figure S2C), but the number of pups born (2.8 ± 0.5 per litter) was consistently lower than that in mice with AS that were administered hPVSCs (6.0 ± 0.4 per litter). Mice with AS that

Figure 1. Murine Model of AS Recapitulates Representative Features of AS in Humans

(A) A schematic diagram to illustrate the induction and observation schedule for a murine model of human AS (n = 5 mice in each group). (B) Masson's trichrome (MT) staining 3, 7, and 14 days after uterine damage to evaluate the degree of the damage. Blue and red colors indicate collagen and cytoplasm, respectively. LE, luminal epithelium; GE, glandular epithelium; S, stroma. Scale bar, 100 μm. (C) Real-time RT-PCR analyses for relative mRNA levels of fibrosis-related factors in uteri with AS. *$p < 0.05$, **$p < 0.01$. (D) Western blotting for COL1A1 and TGF-β1 proteins in AS uteri after damage. GAPDH was used as a loading control. (E) Comparison of MT staining and immunofluorescence (IF) staining of COL1A1 in endometrial tissues from normal controls and AS patients (n = 3 patients in each group) and from AS uteri in mice. Scale bar, 100 μm.

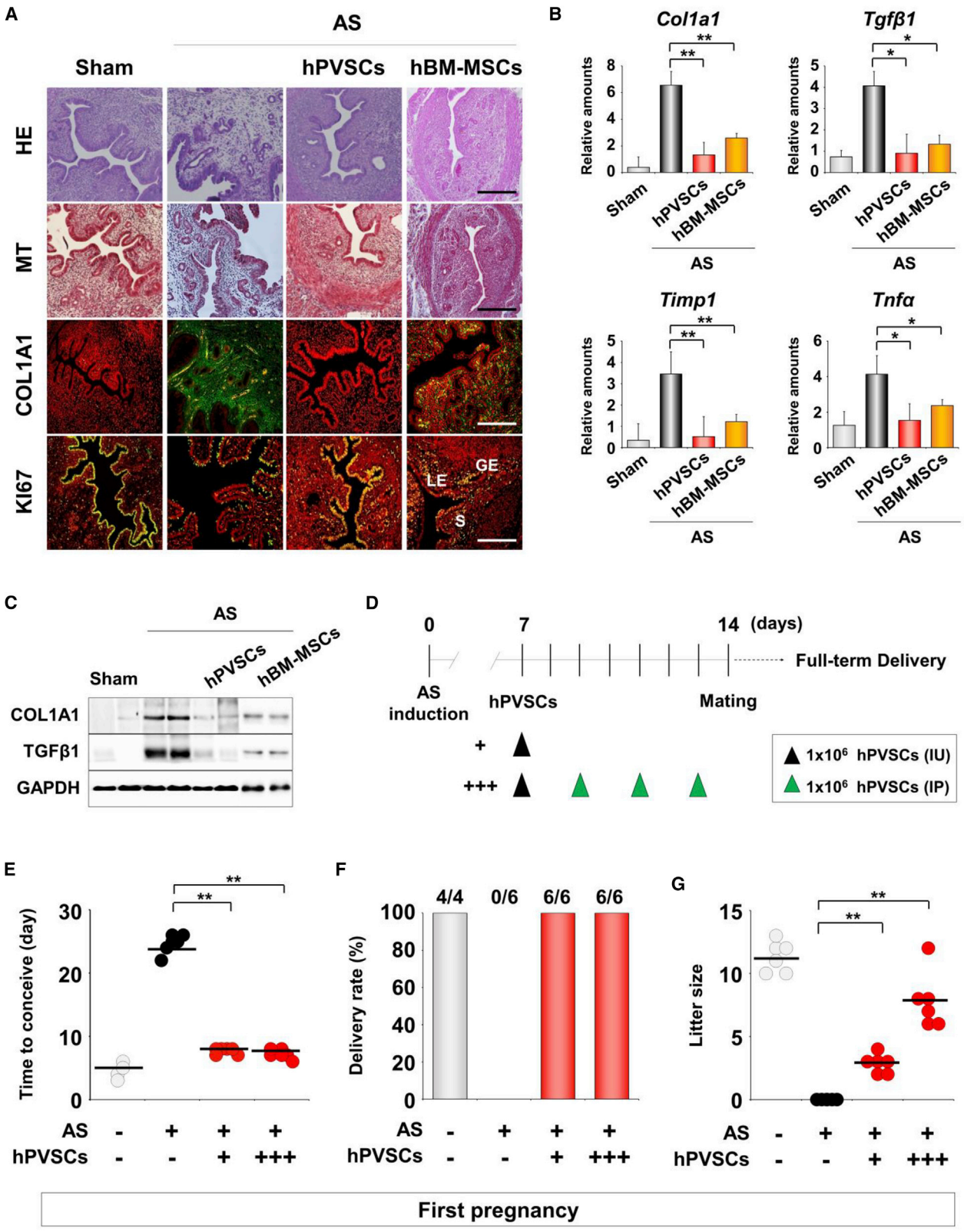

(legend on next page)

were administered hPVSCs showed dose-dependent improvements in pregnancy outcomes that almost reached the levels of the controls (Figure S2D).

hPVSCs Improve Compromised Uterine Environments for Timely Embryo Implantation to Subsequent Fetal Development in Mice with AS

Recent studies have suggested that AS may cause infertility, miscarriage, and placental abnormalities.[7] This could be due to a suboptimal uterine environment that may not support timely embryo implantation, leading to defective fetal development, including IUGR followed by miscarriage.[25] Successful embryo implantation occurs around midnight on day 4.5 in mice,[26] so embryo implantation in mice with AS was examined on day 5 (Figure 3A). Blastocysts failed to implant in mice with AS even on day 5, whereas distinct implantation sites (IS) (shown as blue spots) were observed in uteri of sham controls. Embryos could implant in AS uteri on day 6, but some failed to develop and were absorbed on day 8 (Figure 3B). Interestingly, embryos were successfully implanted on day 5 in the uterine horn treated with hPVSCs, but not in the other horn of mice with AS (Figure 3C). Blastocysts that failed to implant were recovered from the uterine horn with AS. Immunohistochemistry for early growth response 1 (EGR1), as a marker of embryo implantation in IS, reinforced that single IU delivery of hPVSCs before pregnancy allowed normal embryo implantation in mice with AS on day 5 (Figure 3D).

To further investigate this phenotype, we examined the number of IS and the weights of embryos and their placentas in AS uteri on day 12. Mice with AS had fewer IS (2.3 ± 0.5 versus 8.8 ± 0.5 IS/horn, $p < 0.01$) with retarded embryos (47.3 ± 3.7 versus 83.7 ± 6.4 mg, $p < 0.01$) compared to controls on day 12. The IU delivery of hPVSCs (1×10^6) significantly increased the number of IS in uteri with AS (3.8 ± 0.5 versus 2.0 ± 0.8 IS/horn, $p < 0.05$) (Figure 3E). Higher numbers of hPVSCs (5×10^6) produced higher numbers of IS than in mice with AS administered 1×10^6 hPVSCs (5.3 ± 0.7 versus 3.8 ± 0.5, $p < 0.01$), suggesting a dose-dependent therapeutic potential of hPVSCs for AS. Furthermore, hPVSCs (5×10^6) effectively improved the IUGR phenotype of embryos in mice with AS (67.9 ± 4.0 versus 47.3 ± 2.9 mg, $p < 0.01$; Figure 3F). These results are consistent with partial but significant restoration of retarded placental development in AS uteri by delivery of 5×10^6 hPVSCs (52.6 ± 3.7 versus 43.0 ± 3.4 mg, $p < 0.05$; Figure 3G).

hPVSCs Promote Uterine Regeneration via HIF1α-Dependent Angiogenesis in AS Uteri

We next examined the mechanism of how hPVSCs promote uterine regeneration in AS uteri at the molecular level. Because MSCs are known to promote angiogenesis in various injured tissues, we first investigated the expression profiles of proangiogenic factors in AS uteri after delivery of hPVSCs. hPVSCs significantly increased the mRNA expression of major angiogenic factors including *Hif1α*, insulin-like growth factor-1 (*Igf-1*), and vascular endothelial growth factor a (*Vegf-a*) (Figure 4A). Furthermore, the observed increase in ANG-1-dependent TIE2 phosphorylation, which is needed for angiogenesis,[27] is consistent with the increased levels of CD31 (an endothelial cell marker) in AS uteri with hPVSCs (Figure 4B). Co-immunofluorescence (coIF) staining of CD31 and KI-67 reinforced that hPVSCs significantly improved angiogenesis in impaired uteri (Figures 4C and 4D). The functional importance of HIF1α-dependent angiogenesis on the restoration of AS uteri was further evaluated by administering pharmacologic modulators of HIF1α activity (Figures 4E and 4F). A single IU administration of an HIF1α inhibitor, echinomycin (EC), dampened the beneficial effects of hPVSCs (1×10^6) on the number of IS (3.75 ± 0.25 versus 3.0 ± 0.4/horn) on day 12. In contrast, administration of an HIF1α stabilizer, dimethyloxalylglycine (DMOG), significantly increased the number of IS and embryo weights in mice with AS. It is critical to mention that combination therapy of hPVSCs with DMOG produced the best pregnancy outcomes. To demonstrate directly that HIF1α-dependent angiogenesis is critical for hPVSCs to promote the functional restoration of uteri with AS, we induced AS in uteri of *Hif1α*-knockout ($Hif1\alpha^{f/f}$; $Amhr2^{cre/+}$) mice, in which *Hif1α* was specifically deleted in the uterine mesenchyme (Figure S3A). Interestingly, we could not observe therapeutic effects of hPVSCs on fibrotic lesions (Figure 4G) and the expression of angiogenic factors (Figure S3B) in AS uteri deficient of HIF1α.

hPVSCs Contribute to the Restoration of Impaired Uterus in a Paracrine Manner

We then examined whether the i.v. delivery of hPVSCs promotes uterine regeneration (Figure 5A). As shown in Figure 5B, not only IU, but also i.v., delivery of hPVSCs significantly repaired fibrosis in AS uteri. To further investigate the mode of action by which hPVSCs affect AS uteri *in vivo*, we pre-labeled hPVSCs with fluorescent superparamagnetic iron oxide (SPIO) nanoparticles containing iron for Prussian blue (PB) staining prior to i.v. delivery.[28] As soon as the SPIO-labeled hPVSCs were intravenously (i.v.) administered,

Figure 2. hPVSCs Act as MSCs to Promote Uterine Restoration in Mice with AS

(A) Comparative histological evaluation in AS uteri after intrauterine delivery of hPVSCs and hBM-MSCs. Endometrial morphology and immunoreactivity of COL1A1 and KI-67 were evaluated by hematoxylin and eosin (H&E) staining, MT staining, and/or IF staining. Green and yellow colors indicate COL1A1 and KI-67-positive cells, respectively; red indicates nuclei in uterine cells. LE, luminal epithelium; GE, glandular epithelium; S, stroma. Scale bar, 50 μm. (B) Real-time RT-PCR for fibrosis-related factors after hPVSCs or hBM-MSCs transplantation. *$p < 0.05$, **$p < 0.01$. (C) Western blotting for COL1A1 and TGFβ1 in AS uteri after hPVSCs or hBM-MSCs transplantation. GAPDH was used as a loading control (n = 4 or 5 mice in each group). (D) A schematic diagram illustrating the experimental procedures to examine the therapeutic effects of hPVSCs on the irregular reproductive cycle and poor pregnancy outcomes in mice with AS. +, IU delivery of hPVSCs (1×10^6); +++, a single IU followed by three i.p. deliveries of hPVSCs (1×10^6). (E–G) Therapeutic effects of PVSCs on time to conceive (E), delivery rate (F), and litter size (G) in the first pregnancies of mice with AS. The horizontal black lines represent median values. Numbers above the bars indicate the number of mice that delivered live pup(s)/total mice examined. **$p < 0.01$.

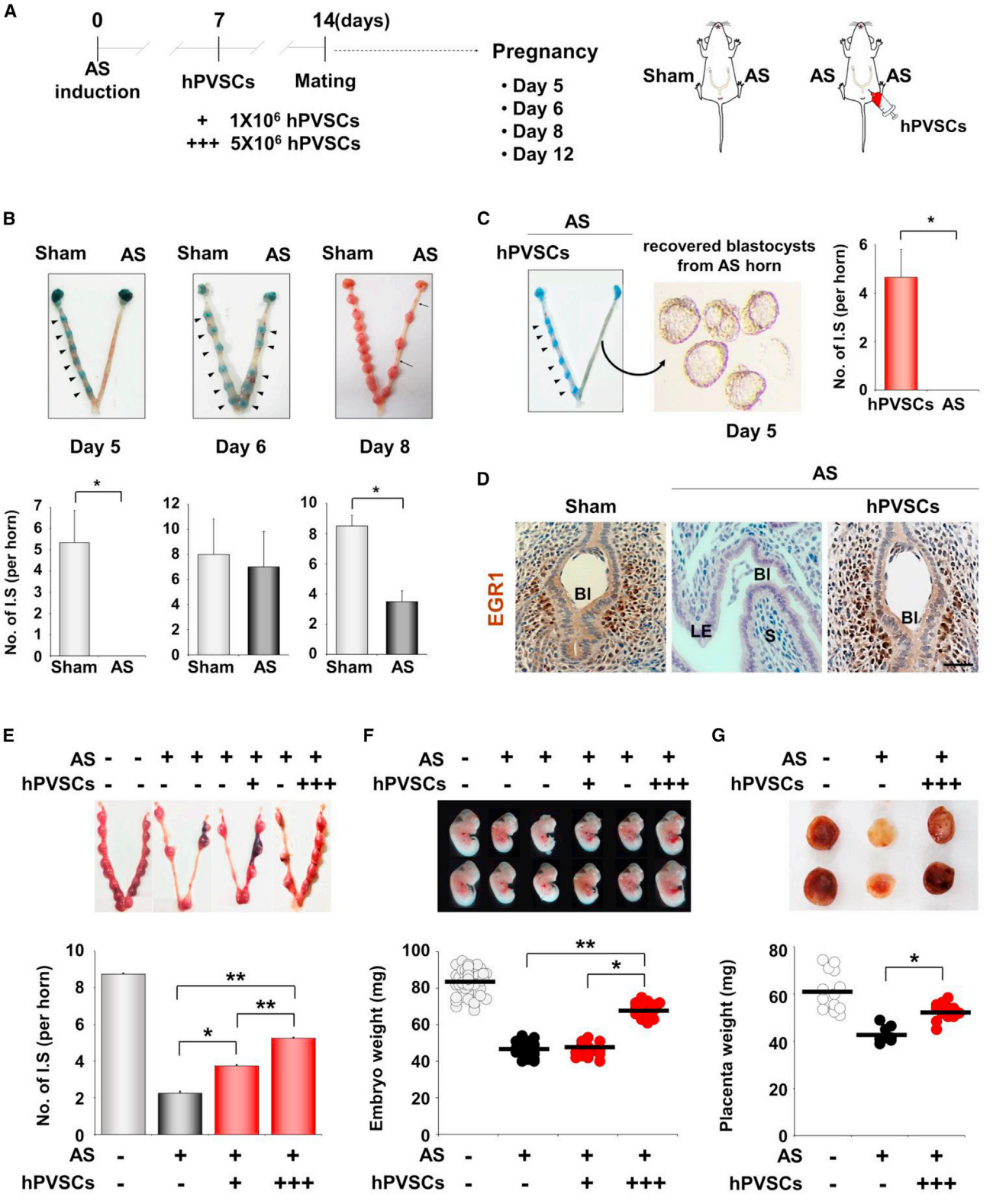

(legend on next page)

fluorescence was immediately observed in highly vascularized tissues, such as spleen, kidney, liver, and female reproductive organs (data not shown). PB staining revealed that iron-positive hPVSCs were similarly detected in both sham and AS uterine horns at 1 and 3 h post-i.v. delivery. However, 6 h after i.v. delivery, significantly higher numbers of PB-positive hPVSCs were detected in the injured uterine horns (12.9% ± 1.8% versus 3.6% ± 1.7%, $p < 0.01$) compared to the sham control horns (Figures 5C and 5D). hPVSCs were found only in AS uteri after 7 days, although the proportion of hPVSCs in uterine horns with AS was sharply decreased to less than 1% (0.458%). These results suggest the homing effects of hPVSCs on the impaired uterus contribute to uterine regeneration in a paracrine manner rather than direct differentiation.

CYP-A Is Secreted from hPVSCs to Facilitate Angiogenesis for Uterine Regeneration in Mice with AS

The results in Figure 5 prompted us to validate the paracrine actions of hPVSCs on the uterus with AS. Medium incubated with hPVSCs (hPVSCs-CM) in a serum-starved condition for 24 h itself had similar positive effects on uterine fibrosis in mice with AS (Figure 6A). Proteomic analyses of hPVSCs-CM were then performed to identify major secreted factor(s) with therapeutic potentials on mice with AS using mass spectrometry. Compared to the culture medium of lung fibroblasts, hPVSCs-CM had several unique spots (Figure 6B). CYP-A was one of top scored proteins that were detected in hPVSCs-CM (Table S1). Whereas CYP-A was barely produced in hPVSCs, hBM-MSCs, and human adipose-derived MSCs under normal culture conditions, it was abundantly produced in hPVSCs and hBM-MSCs under the serum-starvation (Figure 6C). Interestingly, CYP-A was predominantly secreted from hPVSCs but not the other MSCs, suggesting that hPVSCs could provide more CYP-A than other MSCs when administered. When recombinant CYP-A (100 ng/mouse) was given to uterine horns with AS via IU delivery, it significantly reduced fibrotic lesions and expression levels of fibrosis-associated factors at protein levels as competent as hPVSCs and hPVSCs-CM (Figures 6A and 6D) although it did not disturb the immune system and cause toxicity in general (Figure S4). coIF of CD31 and KI67 showed that CYP-A is as effective as hPVSCs at facilitating endothelial cell proliferation in the uterus with AS (Figures 6E and 6F). Furthermore, western blotting showed that CYP-A, as well as hPVSCs, promoted expression of proangiogenic factors including HIF1α and ANG-1, and phosphorylation of TIE2 in the uterus with AS (Figure 6G), suggesting that hPVSCs secrete CYP-A to facilitate HIF1α-dependent angiogenesis for uterine restoration in mice with AS.

DISCUSSION

MSC therapies have been applied to restore and improve the function of the endometrium in patients with AS.[23,29–31] To understand the underlying mechanisms of beneficial effects of MSCs on impaired endometrium in patients with AS, the uteri of mice or rats were physically[32] or chemically[33,34] traumatized. While these previous studies suggest that MSCs facilitate the expression of genes involved in cell proliferation and uterine receptivity, and fertility in these murine models,[28,32,35] it is still unclear whether they share the same pathophysiologic features of human patients with AS. We provide evidence to support the idea that a physically traumatized mouse model of AS recapitulates the major reproductive disturbances of human patients with AS, including oligo-/amenorrhea, IUGR, and miscarriage (Figures 2 and 3). Histologically, the human endometrium in patients with AS is observed to form dense fibrous strips and tends to increase in thickness.[19] In addition, its increased expression levels of *collagen 1* and *Tgfβ1* favor firm adhesion formation,[36] all of which were similarly observed in our mouse model of AS (Figure 1).

Unsynchronized and/or improper interactions between the embryo and the endometrium can make embryo implantation untimely delayed, which can lead to pregnancy loss in both humans[37] and mice.[38] In humans, patients with AS also tend to have a higher risk of IUGR during pregnancy compared to women with a healthy endometrium.[24,39] IUGR occurs as a result of suboptimal fetal growth, accompanied by an increased risk of neonatal morbidity.[40] In fact, we observed a gradual decrease in the number of fetuses during the progression of pregnancy and subsequent delivery failures in mice with AS (Figure 3B). For the first time, we demonstrated that AS uteri cannot provide a favorable environment to support successful embryo implantation followed by postimplantation fetal development (Figure 3). These data suggest that infertility of patients with AS may come, at least in part, from poor embryo implantation.[39] The administration of hPVSCs before pregnancy significantly recovered compromised uterine milieu for embryo implantation (Figure 3), suggesting a possibility that MSC therapy may help patients who suffer from repeated implantation failure and recurrent spontaneous abortion, as well as AS.

Angiogenesis is an important step in wound healing during menstruation.[41] HIF1α-dependent hypoxia is required for endometrial repair after menstruation in humans and in a mouse model of simulated menses.[42] Defective angiogenesis is strongly associated with poor decidualization and could be a possible cause of recurrent pregnancy loss.[43] Our results show that the expression of angiogenesis-related

Figure 3. hPVSCs Improve Compromised Uterine Environments for Embryo Implantation and Subsequent Developments in Mice with AS

(A) The number of implantation sites (ISs) were observed on days 5, 6, 8, and 12 of pregnancy (days 5, 6, 8, and 12; n = 4 or 5 mice in each group). +, IU delivery of hPVSCs (1×10^6), +++, IU delivery of hPVSCs (5×10^6). (B) Representative images of uteri with or without ISs in mice with AS on different days of pregnancy (days 5, 6, and 8). On day 5, ISs were not observed in mice with AS and unimplanted blastocysts were harvested. Embryo implantation did occur in these mice on day 6. Arrowheads indicate the ISs. On day 8, ISs were decreased in mice with AS and sites of spontaneous abortion were harvested (arrows). (C) The number of ISs in mice with AS on days 5, 6, and 8. Numbers above the bars indicate the number of mice with ISs/total mice examined. (D) Immunohistochemical staining of EGR1 for ISs on day 5. (E) The number of ISs observed on day 12. (F) Representative images of embryos and a distribution graph of weights of embryos collected from ISs on day 12. (G) Placental histology and weight distribution of ISs on day 12. The horizontal black lines represent the median values of weights of embryos (F) and their placentas (G). *$p < 0.05$, **$p < 0.01$.

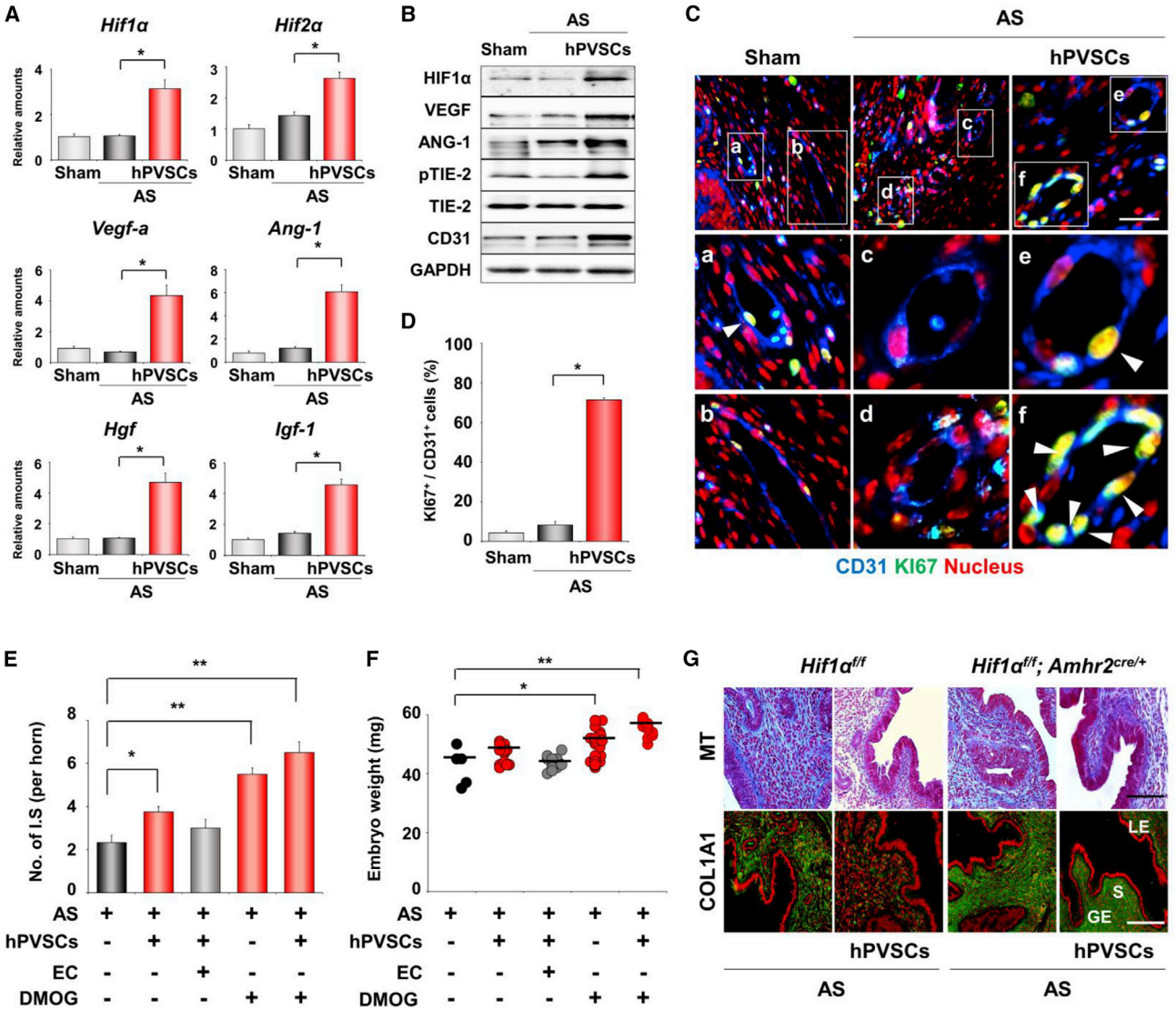

Figure 4. hPVSCs Facilitate HIF1α-Dependent Angiogenesis to Improve Fertility in Mice with AS

(A) Real-time RT-PCR of angiogenesis-related factors after hPVSCs transplantation. (B) Western blotting for HIF1α, VEGF-A, ANG1, phosphorylated TIE-2 (pTIE-2), and CD31 protein in uteri after hPVSCs transplantation. GAPDH was used as a loading control. (C) Co-immunofluoresence (coIF) staining of CD31 and KI-67 in uteri 7 days after hPVSCs transplantation. Blue, green, and red colors indicate CD31, KI-67, and nuclei, respectively. White arrowheads indicate proliferating endothelial cells (yellow nuclei). Scale bar, 50 μm. (D) Quantification of results in (C). (E and F) Improvement of pregnancy outcomes in mice with AS by administration of a HIF1α stabilizer (DMOG) on day 12. Graphs of the number of ISs (E) and embryo weights (F) on day 12 (n = 6–8 mice in each group). HIF1α inhibitor, EC. The statistical significance of each group was evaluated with AS group. *$p < 0.05$, **$p < 0.01$. (G) MT staining and IF staining of COL1A1 in AS uteri of uterine-specific *Hif1α*-knockout (*Hif1α*$^{f/f}$; *Amhr2*$^{cre/+}$) mice after hPVSCs transplantation (n = 3 mice in each group). Green and red colors in the upper images indicate COL1A1 and nuclei, respectively. LE, luminal epithelium; GE, glandular epithelium; S, stroma. Scale bar, 50 μm.

factors was significantly increased in mice with AS after hPVSCs therapy (Figures 4A and 4B). We also recently demonstrated that embryonic stem cell-derived MSCs promote their expression in AS uteri.[44] In addition, hPVSCs overexpressing CYR61 promoted vascular development and provided better restorative effects than parental hPVSCs in rat models of partial uterine excision.[21] However, these previous studies did not provide direct evidence that angiogenesis is a prerequisite for endometrial restoration in cases of AS. We found that the administration of DMOG, a PHD inhibitor that stabilizes HIF1α even under normoxic conditions,[42] significantly improved endometrial function during pregnancy in the absence of hPVSCs (Figures 4E and 4F). This result suggests that the modulation of HIF1α itself could be a treatment option for human patients with severe AS. Additionally, the transplantation of hypoxia-preconditioned

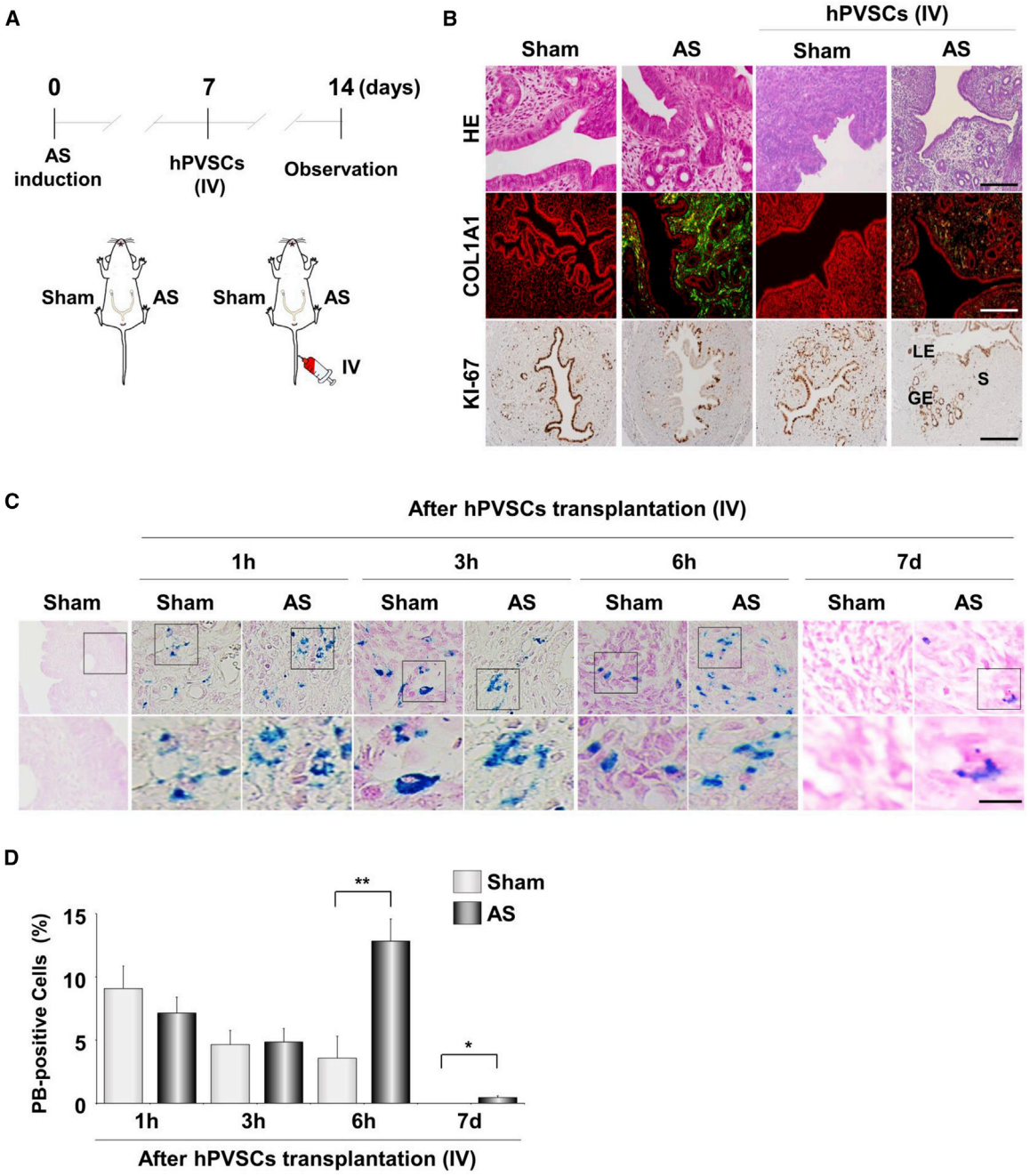

Figure 5. hPVSCs Contribute to Uterine Regeneration in a Paracrine Fashion

(A) A schematic diagram illustrating the experimental procedures for the intravenous (i.v.) delivery of hPVSCs to mice with AS. AS was induced in one uterine horn while the other horn served as the sham control in the same mouse (n = 4–6 mice in each group). (B) Observation of the antifibrotic functions of hPVSCs delivered i.v. into uteri with AS. Gross histology with H&E staining and IF staining of COL1A1 and immunohistochemical staining of KI-67 in uteri with AS after i.v. delivery of hPVSCs. Green and red colors indicate COL1A1 and nuclei, respectively. Brown indicates KI-67-positive uterine cells. LE, luminal epithelium; GE, glandular epithelium; S, stroma, Scale bar, 100 μm. (C) Prussian blue (PB) staining of iron deposits to track hPVSCs in the uterus after i.v. delivery. Scale bar, 25 μm. (D) Quantitation of PB-positive hPVSCs in the uterus after i.v. delivery. *$p < 0.05$, **$p < 0.01$.

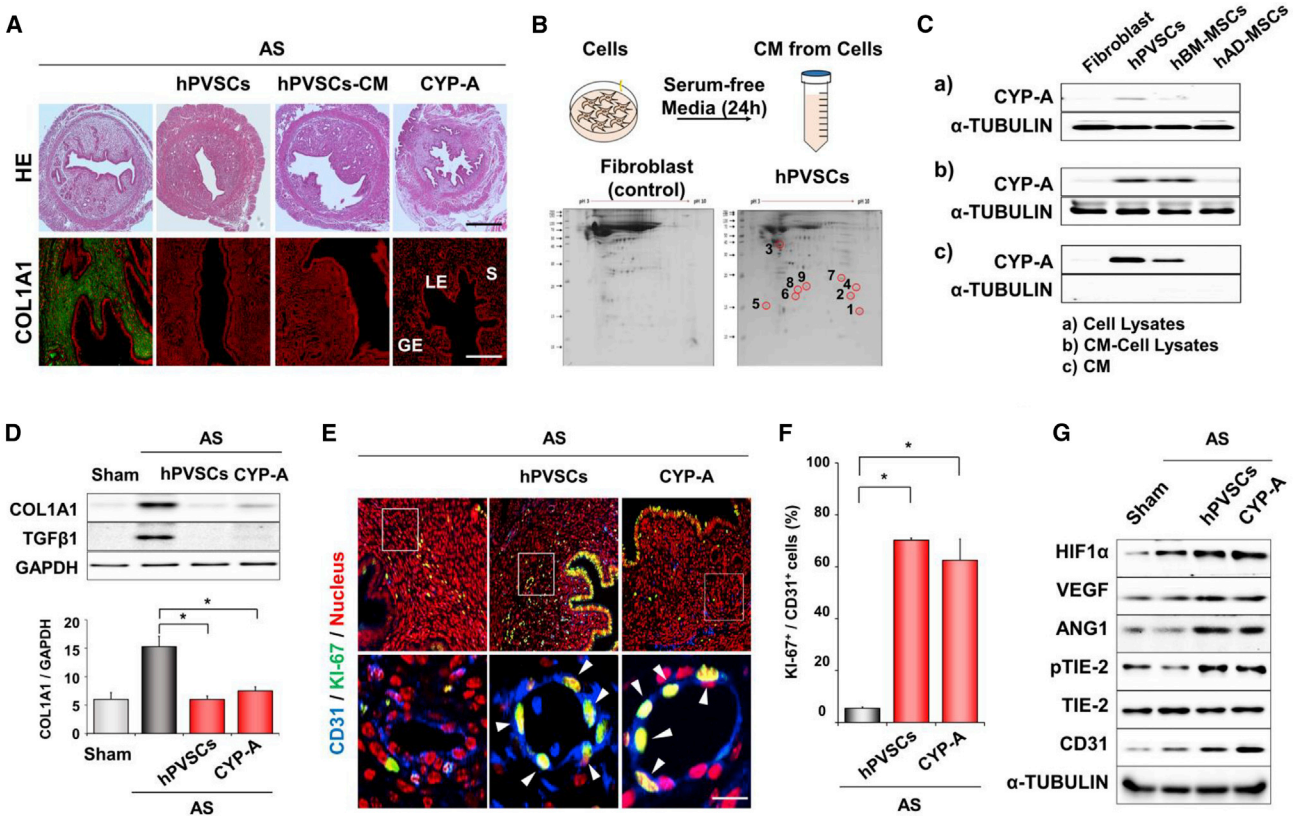

Figure 6. CYP-A Secreted from hPVSCs Contributes Major Therapeutic Actions of hPVSCs on Uterine Restoration in Mice with AS

(A) Gross histology (H&E) and IF staining for COL1A1 in uterine sections of mice with AS after intrauterine delivery of hPVSCs, concentrated conditioned medium (CM) of hPVSCs, and CYP-A. Scale bar, 100 μm. (B) A schematic diagram and gel images of 2D electrophoresis of experiments with CM from hPVSCs and human lung fibroblasts. CM was harvested after being incubated with cells in a serum-starved condition for 24 h. CM from hPVSCs had several unique spots compared to CM of lung fibroblasts (numbers 1 to 9). (C) Western blotting for CYP-A in cells incubated under serum-contained (a) and -starved conditions (b), respectively, and CM (c) of (b). Note that CYP-A is predominantly secreted from hPVSCs among MSCs tested. (D) Representative images of western blotting and graphs for COL1A1 and TGF-β1 protein in mice with AS after CYP-A treatment (n = 4 or 5 mice in each group). *$p < 0.05$. (E) coIF staining for CD31 and KI-67 in mice with AS after CYP-A treatment. Blue, green, and red colors indicate CD31, KI-67, and nucleus, respectively. White arrows indicate KI-67 positive nuclei (yellow color) in endothelial cells. Scale bar, 25 μm. (F) Graphs depicting the percentage of KI-67 positive cells/CD31 positive cells counted. *$p < 0.05$. (G) Western blotting for HIF1α, VEGF-A, ANG1, TIE-2, pTIE-2, and CD31 in mice with AS after CYP-A treatment. Note that CYP-A treatment itself significantly increases the expression of all angiogenesis-related factors tested in mice with AS (n = 6–8 mice in each group). Green and red colors indicate COL1A1 and nucleus, respectively in (A) and (D). LE, luminal epithelial cells; GE, glandular epithelial cells; S, stromal cells.

MSCs exerted better therapeutic effects in mice with pulmonary fibrosis and enhanced the survival rate of engrafted MSCs.[45] No therapeutic effects of hPVSCs on the uterus of *Hif1α$^{f/f}$; Amhr2$^{cre/+}$* mice (Figure 4G) clearly reinforces the hypothesis that HIF1α-dependent angiogenesis is critical for uterine regeneration facilitated by MSCs during physiologic and/or pathologic hypoxia.

The systemic i.v. delivery of BM-MSCs or uterine-derived cells provided better engraftment than local IU delivery in the injured uterine horn.[46] However, a difference between systemic i.v. and local IU deliveries of hPVSCs was not observed in this study (Figures 2 and 5). Furthermore, i.p. delivery contributed to the morphologic and functional restoration of injured uteri as well (data not shown). Although transplanted BM-MSCs migrate to the injured endometrium and differentiate into endometrial cells, the number of colonized MSCs at the site of injury was disappointingly low (~0.4% in the uterine horn).[3,28] These reports are consistent with our observation (Figure 5), suggesting that the major contribution of MSCs is transient and without efficient integration into the injured endometrium. Thus, beneficial effects of MSCs appear to be elicited in a paracrine manner.[47–49] MSCs secrete various growth factors and cytokines and could transfer exosomes to the injured tissue.[50] Exosomes from BM-MSCs may also promote the repair of injured endometria, similar to the effects of BM-MSCs in rabbits.[51] In CM of BM-MSCs, several factors were identified as important regulators of angiogenesis, including IGF-1 and VEGFs.[52] Proteomic analyses of hPVSCs secretome identified CYP-A as a paracrine factor secreted from hPVSCs to promote HIF1α-dependent angiogenesis in mice with AS (Figure 6). It should be noted that CYP-A promoted expression of all key angiogenic factors, as well as functional restoration of the uterus with AS,

suggesting that CYP-A may act as a primary regulator of uterine regeneration.

CYP-A was initially known as an intracellular binding protein of the immunosuppressive drug cyclosporine A. CYP-A has an activity of peptidylprolyl *cis-trans* isomerase, which contributes to diverse functions, including immune-modulation, cell signaling, and protein folding and trafficking.[53] In addition to the intracellular roles, CYP-A can be secreted as extracellular CYP-A (eCYP-A) to show unique functions in response to various stimuli, such as inflammation, vascular injury, and hypoxia *in vivo*.[54] Although eCYP-A is a proinflammatory cytokine that promotes inflammation and has a chemotactic effect on immune cells, such as monocytes and macrophages,[55] the biosafety of the concentration of CYP-A (5 mg/kg) used in this study is assured by a recent study[56] and Figure S4. eCYP-A is a novel paracrine and autocrine modulator of endothelial cells in immune-mediated vascular diseases.[57] Contribution of CYP-A to vascular remodeling was clearly shown in CYP-A knockout mice and vascular smooth muscle cell (VMSC)-specific CYP-A overexpression mice, where proliferation of VSMC was decreased and increased, respectively.[58]

CYP-A is remarkably overexpressed in multiple types of cancers including lung, liver, and endometrial cancers. A recent study suggests that CYP-A is upregulated by HIF1α in pancreatic ductal adenocarcinoma.[59] Moreover, chromatin immunoprecipitation analysis shows that HIF1α can directly bind to the hypoxia response element in the CYP-A promoter regions and regulate CYP-A expression. Interestingly, another peptidylprolyl *cis-trans* isomerase, PIN1, directly binds to and stabilizes HIF1α,[60] suggesting a possibility of positive feedback mechanisms between CYP-A and HIF1α for angiogenesis in the uterus with AS. CYP-A promotes the recruitment of BM-derived $CD117^+$ cells to tissues with ischemic injury.[61] We showed that hPVSCs secrete eCYP-A and administration of recombinant CYP-A increased promoted HIF1α-dependent angiogenesis. Thus, CYP-A derived from exogenous MSCs may facilitate the homing effect of endogenous BM-derived cells to the injured uterus with AS to amplify signals required for uterine regeneration. Further studies are strongly needed to evaluate the underlying mechanism of the therapeutic actions of hPVSCs-derived CYP-A. In conclusion, we demonstrate that hPVSCs secrete CYP-A to facilitate HIF1α-dependent angiogenesis, which is a prerequisite to correct compromised uterine environment for timely embryo implantation and subsequent complications associated with AS such as IUGR, spontaneous abortion, and miscarriage.

MATERIALS AND METHODS

Mice

All mice used in this study were housed in the Animal Care Facility of CHA University, according to the institutional guidelines for laboratory animals. This study was approved by the Institutional Animal Care and Use Committee of CHA University (approval number 160100). All mice were housed under temperature- and light-controlled conditions (12-h light:dark cycle) and fed *ad libitum*. $Hif1\alpha^{f/f}$ mice were initially generated by Randall Johnson (UC-San Diego Institute, CA, USA) and provided by the Jackson Laboratory (Bar Harbor, ME, USA). $Amhr2^{cre/+}$ mice were generously provided by Dr. Richard Behringer (MD Anderson Cancer Center, TX, USA). Genotyping PCR was performed using genomic DNA extracts from mouse tail biopsies with specific primers (Table S2). Female reproductive tract-specific *Hif1α*-knockout mice ($Hif1\alpha^{f/f}$; $Amhr2^{cre/+}$) were produced by breeding $Hif1\alpha^{f/f}$ mice with $Amhr2^{cre/+}$ mice.

Experimentally Induced Murine Model of AS

Eight-week-old ICR female mice, provided by KOATECH (Pyeongtaek, Gyeonggi, Korea) were used to induce a mouse model of AS, as previously described with minor modifications.[32] After administration of avertin by i.p. injection, a vertical incision was made in the abdominal wall, and the uterus was exposed. A small incision was made in each uterine horn at the uterotubal junction, and the horn was traumatized in a standardized fashion using a 27-gauge needle inserted through the lumen, which was rotated and withdrawn 10 times. For cell transplantation, cells were directly injected into mice with AS after 7 days. After cell transplantation in mice with AS, the assessment of the therapeutic effects was carried out at day 14.

Human Sample

MT and IF staining of human samples were performed using stored human endometrial tissues, diagnosed as severe IUA or normal after hysteroscopy, in the Department of Pathology of CHA Gangnam Medical Center. This study was approved by the Institutional Review Board (IRB approval number, GCI-19-12) of the CHA Gangnam Medical Center.

Isolation and Culture of hUC-PVSCs

hUC tissues were obtained from full-term births after Caesarian sections with informed consent according to the guidelines approved by the IRB at Kangwon National University Hospital (IRB approval number: KNUH-2012-11-003-008). hUC-PVSCs were isolated and cultured, as previously described.[62]

Flow Cytometry

Single-cell suspensions were harvested from hUC-PVSCs cultures by dissociation with 0.05% trypsin-EDTA and resuspended in 3% FBS/PBS. The cells were filtered through a 70-μm filter and incubated for 1 h at 4°C with the following fluorochrome-conjugated mouse anti-human antibodies (1:1,000): CD34-fluorescein-isothiocyanate (FITC), CD31-phycoerythrin (PE), CD45-allophycoerythrin (APC), CD146-FITC, SSEA-4-FITC, CD44-APC, and CD90-APC (all BD Biosciences, San Jose, CA, USA). Nonspecific immunoglobulin Gs (IgGs) of the corresponding cells served as the negative controls. After being immunoassayed, the cells were stained with 7-amino actinomycin to exclude dead cells. Flow cytometric analysis was performed using an Accuri C6 instrument (BD Biosciences), and acquired data were analyzed using FlowJo software (Tree Star, Ashland, OR, USA).

Multilineage Differentiation of hUC-PVSCs

The multilineage differentiation potential of hUC-PVSCs was evaluated, and the medium was changed every 3 days unless otherwise indicated for all differentiation assays as previously described.[62]

SPIO Labeling of hUC-PVSCs

A nontransfection-based method using SPIO (Molday ION Rhodamine B; CL-50Q02-6A-50, 2 mg Fe/mL; BioPAL, Worcester, MA, USA) was used to label hUC-PVSCs prior to transplantation into mice. SPIO was added to the supplemented medium at a concentration of 50 μg/mL, and cells were incubated for 18 h. The images of fluorescent tissues were obtained with Pearl Impulse animal imaging system (LI-COR Biosciences, Lincoln, NE, USA). Cell engraftment was assessed by intracellular iron deposit visualization after treatment with SPIO using PB Iron Stain Kit (HT20; Sigma-Aldrich, St. Louis, MO, USA). The spleens of untreated mice were used as positive controls, and lungs were used as negative controls for iron deposits.

Preparation of Conditioned Medium of MSCs

MSCs conditioned media (MSCs-CM) were prepared following a previously described protocol.[63] To prepare MSCs-CM, we grew MSCs (passage 1 to 3) to 80%–90% confluency in 75T culture flasks using 10% FBS supplemented complete MEMα media. After they were attached, the MSCs were washed once with PBS and twice with serum-free MEMα (SF-MEMα) to remove any serum and switched to SF-MEMα. MSCs were conditioned by exposing SF-MEMα on 80%–90% confluent MSCs for 24 h under a standard culture condition. The resultant medium was collected, centrifuged at 500 × *g* for 5 min, and filtered through 0.22 μm syringe filter (Millipore, Burlington, MA, USA) as previously described[64] to remove any cell debris. The filtered media were concentrated by ultrafiltration using 3-kDa cutoff ultrafiltration membrane (Millipore) and protein concentration was measured by bicinchoninic acid (BCA) assay (Thermo Fisher Scientific, Waltham, MA, USA). The filtrate was used in subsequent experiments as CM.

Mass Spectrometry

To perform the liquid chromatography-tandem mass spectrometry (LC-MS/MS), we determined MSCs-CMs with by Bradford assay. Samples (500 μg) were applied to Immobiline Drystrips gels (pH 4–7, 18 cm, Amersham, Little Chalfont, UK) as a first dimension of 2D electrophoresis. The second separation was performed on 7.5%–17.5% linear gradient polyacrylamide gels. The gels were fixed with 40% methanol containing 5% phosphoric acid for 12 h and then stained with colloidal Coomassie blue (Novex, San Diego, CA, USA) for 48 h. Molecular mass was determined with a 10–200 kDa standard protein marker (GIBCO, Basel, Switzerland) on the right side of select gels. The gels were then destained with water, scanned using a GS-800 imaging densitometer (Bio-Rad), and the images analyzed with PDQuest software (Bio-Rad). Matrix-assisted laser desorption ionization time-of-flight (MALDI-TOF) analysis was used to identify protein bands (ProteomTech, Seoul, Korea).

Histological Staining

The 4% PFA-fixed, paraffin-embedded uterine tissues were sectioned and stained with hematoxylin and eosin (H&E) and MT. Uterine sections (5 μm) were deparaffinized and rehydrated. Endogenous peroxidase was inactivated with 3% H_2O_2. Sections were subjected to antigen retrieval in 0.01 M sodium citrate buffer (pH 6.0). Nonspecific staining was blocked using protein block serum (Dako, Carpinteria, CA, USA). Sections were then incubated with primary antibody at 4°C overnight. To confirm fibrosis in AS tissues, we performed anti-COL1A1 (NB600-408, 1:200; Novus Biologicals, Charles, MO, USA) staining. Angiogenesis was confirmed using anti-KI-67 antibody (ab16667, 1:200; Abcam, Cambridge, UK), and anti-CD31 (553370, 1:200; BD Bioscience). Uterine cells positive for CD31, KI-67, and DAPI were counted. For statistical analysis, the capillary density (number of $CD31^+$ blood vessels and $KI\text{-}67^+$ nuclei) was calculated from at least 10 randomly selected fields of eight uteri. The next morning, sections were incubated with secondary antibody for 1 h at room temperature. After three washes in PBS, sections were counterstained and mounted. Images were obtained for microscopy (Carl Zeiss, Oberkochen, Germany) and analyzed using ZEN software (Carl Zeiss).

RNA Preparation, RT-PCR, and Real-Time RT-PCR

Total RNA was extracted from each uterine tissue using the Trizol reagent (Ambion, Carlsbad, CA, USA), according to the manufacturer's protocol. Two μg of uterine total RNA was subjected to reverse transcription (RT) using M-MLV reverse transcriptase (Promega, Madison, WI, USA) with random primers and the oligo dT primer for cDNA synthesis. Synthesized cDNA was utilized for PCR with specific primers at optimized cycles (Table S3). For quantification of expression levels, real-time RT-PCR was performed using the SYBR green dye (iQ SYBR Green Supermix, Bio-Rad, Waltham, MA, USA), as previously described.[65,66] For comparison of transcript levels between samples, a standard curve of cycle thresholds for several serial dilutions of a cDNA sample was established and then used to calculate the relative abundance of each gene. Values were then normalized to the relative amounts of *Rpl7* cDNA. All reactions were performed in duplicate.

Western Blotting

Tissues were lysed in lysis buffer including PRO-PREP (iNtRON, Seongnam, Korea) and 1× phosphatase inhibitor (Roche Applied Science, Indianapolis, IN, USA). The protein samples (20 μg/lane) were then separated by 6%–15% SDS-PAGE, transferred onto a nitrocellulose membrane (Bio-Rad), and blocked with 5% non-fat milk (Bio-Rad) in TBS (Bio-Rad) containing 0.1% Tween 20 (Sigma-Aldrich). Anti-collagen type I (Novus), anti-TGF-β1 (sc-130348, 1:1,000; Santa Cruz, Dallas, TX, USA), anti-HIF1α (NB100-479, 1:1,000; Novus), anti-VEGF (ab46154, 1:1,000; Abcam), anti-ANG-1 (MAB8220, 1:1,000; R&D Systems, Minneapolis, MN, USA), anti-pTIE-2 (AF3909, 1:1,000; R&D Systems), anti-TIE-2 (AF762, 1:1,000; R&D Systems), anti-CD31 (BD Biosciences), anti-tubulin alpha (T9026, 1:3,000; Sigma-Aldrich), and anti-GAPDH (#2118, 1:3,000; Cell Signaling, Danvers, MA, USA) were used for western blotting

analysis. The signals were developed using the ECL WB substrate kit (Bio-Rad) and detected using Chemidoc XRS+ (Bio-Rad) with image lab software.

Analyses of Embryo Implantation and Pregnancy Outcomes

Pregnancy was evaluated by the presence of a vaginal plug on the next morning after breeding with a fertile male. Implantation sites (ISs) were visualized by the i.v. injection of a Chicago blue dye solution (1% in PBS) on days 5 and 6 of pregnancy (days 5 and 6),[50] and the number of IS demarcated by distinct blue bands was recorded. The uteri of mice without ISs were flushed with medium to recover unimplanted blastocysts. Recovered embryos were observed under a dissecting microscope. ISs and embryos on days 8 and 12 were examined, as previously described, with some modifications.[38] Isolated day 12 ISs were weighed individually, fixed in 4% PFA overnight, and dissected to isolate the embryo and the placenta. Isolated embryos and placentas were weighed individually, and their images were captured to examine their size and gross morphology. To evaluate reproductive performance, mice with AS, with or without transplantation of hPVSCs, were individually bred with fertile males. The numbers of pups in each litter were recorded.

Pharmacological Modulators of HIF1α

Echinomycin (EC; HIF1α inhibitor, 1 mg/kg, Bioviotica, Liestal, Switzerland) or dimethyloxalylglycine (DMOG; PHD inhibitor; HIF1α stabilizer; 8 mg, Enzo Life Sciences, Lausen, Switzerland) was used to either inhibit or stabilize HIF1α activity in mice with AS, respectively.

Recombinant Human Protein CYP-A

CYP-A (5 mg/kg; 100 ng/mouse, ProSpec, Ness-Ziona, Israel) was locally delivered into the uterine horn(s) in mice with AS.

Evaluation of Immune Cell Profiles and General Toxicity after Intrauterine Delivery of CYP-A

Whole blood was withdrawn 24 h after intrauterine delivery of PBS or CYP-A (100 ng) into mice. Immune cell profiles and general toxicity were immediately evaluated in these blood samples as described previously.[56]

Statistical Analysis

All values represent the mean ± SD. Statistical analyses were performed using the Mann-Whitney U test for comparisons between two groups and the Kruskal-Wallis ANOVA test for more than two groups. Values of p less than 0.05 were considered statistically significant. GraphPad Prism version 5 software (GraphPad Software, La Jolla, CA, USA) was used for statistical analyses.

SUPPLEMENTAL INFORMATION

Supplemental Information can be found online at https://doi.org/10.1016/j.ymthe.2020.05.015.

AUTHOR CONTRIBUTIONS

Conceptualization, M.P., S.-H.H., S.W.L., and H.S.; Methodology, M.P., S.-H.H., S.H.P., Y.S.K., S.C.Y., H.-R.K., S. Noh, S. Na, H.K.L., and H.J.L.; Investigation, M.P., S.-H.H., S.H.P., Y.S.K., S.C.Y., H.-R.K., S. Noh, S. Na, H.K.L., and H.J.L.; Writing – Original Draft, M.P., S.-H.H., S.W.L, and H.S.; Funding Acquisition, S.W.L., and H.S.; Supervision, S.W.L., and H.S.

CONFLICTS OF INTEREST

The authors declare no competing interests.

ACKNOWLEDGMENTS

This research was supported in part by a grant of the Korean Health Technology R&D Project through the Korea Health Industry Development Institute (KHIDI) funded by the Ministry of Health & Welfare, Republic of Korea (HI17C1133 to H.S.); grants from the National Research Foundation of Korea (NRF) funded by the Korean government (NRF-2016R1C1B1014281 to S.W.L. and NRF- 2020R1A2C2005012 to H.S.); and Basic Science Research Program through the National Research Foundation of Korea (NRF) funded by the Ministry of Education (NRF-2019R1A6A1A03032888).

REFERENCES

1. Choi, Y., Kim, H.R., Lim, E.J., Park, M., Yoon, J.A., Kim, Y.S., Kim, E.K., Shin, J.E., Kim, J.H., Kwon, H., et al. (2016). Integrative Analyses of Uterine Transcriptome and MicroRNAome Reveal Compromised LIF-STAT3 Signaling and Progesterone Response in the Endometrium of Patients with Recurrent/Repeated Implantation Failure (RIF). PLoS ONE *11*, e0157696.
2. Gargett, C.E., and Healy, D.L. (2011). Generating receptive endometrium in Asherman's syndrome. J. Hum. Reprod. Sci. *4*, 49–52.
3. Sahin Ersoy, G., Zolbin, M.M., Cosar, E., Moridi, I., Mamillapalli, R., and Taylor, H.S. (2017). CXCL12 Promotes Stem Cell Recruitment and Uterine Repair after Injury in Asherman's Syndrome. Mol. Ther. Methods Clin. Dev. *4*, 169–177.
4. Gargett, C.E., Nguyen, H.P., and Ye, L. (2012). Endometrial regeneration and endometrial stem/progenitor cells. Rev. Endocr. Metab. Disord. *13*, 235–251.
5. Mutlu, L., Hufnagel, D., and Taylor, H.S. (2015). The endometrium as a source of mesenchymal stem cells for regenerative medicine. Biol. Reprod. *92*, 138.
6. Yu, D., Wong, Y.M., Cheong, Y., Xia, E., and Li, T.C. (2008). Asherman syndrome–one century later. Fertil. Steril. *89*, 759–779.
7. Conforti, A., Alviggi, C., Mollo, A., De Placido, G., and Magos, A. (2013). The management of Asherman syndrome: a review of literature. Reprod. Biol. Endocrinol. *11*, 118.
8. Deans, R., and Abbott, J. (2010). Review of intrauterine adhesions. J. Minim. Invasive Gynecol. *17*, 555–569.
9. Lebovitz, O., and Orvieto, R. (2014). Treating patients with "thin" endometrium - an ongoing challenge. Gynecol. Endocrinol. *30*, 409–414.
10. Azizi, R., Aghebati-Maleki, L., Nouri, M., Marofi, F., Negargar, S., and Yousefi, M. (2018). Stem cell therapy in Asherman syndrome and thin endometrium: Stem cell- based therapy. Biomed. Pharmacother. *102*, 333–343.
11. Wang, X., Ma, N., Sun, Q., Huang, C., Liu, Y., and Luo, X. (2017). Elevated NF-κB signaling in Asherman syndrome patients and animal models. Oncotarget *8*, 15399–15406.
12. Klingemann, H., Matzilevich, D., and Marchand, J. (2008). Mesenchymal Stem Cells - Sources and Clinical Applications. Transfus. Med. Hemother. *35*, 272–277.
13. Mueller, S.M., and Glowacki, J. (2001). Age-related decline in the osteogenic potential of human bone marrow cells cultured in three-dimensional collagen sponges. J. Cell. Biochem. *82*, 583–590.

14. Watson, N., Divers, R., Kedar, R., Mehindru, A., Mehindru, A., Borlongan, M.C., and Borlongan, C.V. (2015). Discarded Wharton jelly of the human umbilical cord: a viable source for mesenchymal stromal cells. Cytotherapy *17*, 18–24.

15. Crisan, M., Yap, S., Casteilla, L., Chen, C.W., Corselli, M., Park, T.S., Andriolo, G., Sun, B., Zheng, B., Zhang, L., et al. (2008). A perivascular origin for mesenchymal stem cells in multiple human organs. Cell Stem Cell *3*, 301–313.

16. Bouacida, A., Rosset, P., Trichet, V., Guilloton, F., Espagnolle, N., Cordonier, T., Heymann, D., Layrolle, P., Sensébé, L., and Deschaseaux, F. (2012). Pericyte-like progenitors show high immaturity and engraftment potential as compared with mesenchymal stem cells. PLoS ONE *7*, e48648.

17. Vieira Paladino, F., de Moraes Rodrigues, J., da Silva, A., and Goldberg, A.C. (2019). The Immunomodulatory Potential of Wharton's Jelly Mesenchymal Stem/Stromal Cells. Stem Cells Int. *2019*, 3548917.

18. Pierro, M., Ionescu, L., Montemurro, T., Vadivel, A., Weissmann, G., Oudit, G., Emery, D., Bodiga, S., Eaton, F., Péault, B., et al. (2013). Short-term, long-term and paracrine effect of human umbilical cord-derived stem cells in lung injury prevention and repair in experimental bronchopulmonary dysplasia. Thorax *68*, 475–484.

19. James, A.W., Zara, J.N., Zhang, X., Askarinam, A., Goyal, R., Chiang, M., Yuan, W., Chang, L., Corselli, M., Shen, J., et al. (2012). Perivascular stem cells: a prospectively purified mesenchymal stem cell population for bone tissue engineering. Stem Cells Transl. Med. *1*, 510–519.

20. Avolio, E., Alvino, V.V., Ghorbel, M.T., and Campagnolo, P. (2017). Perivascular cells and tissue engineering: Current applications and untapped potential. Pharmacol. Ther. *171*, 83–92.

21. Li, Z., Yan, G., Diao, Q., Yu, F., Li, X., Sheng, X., Liu, Y., Dai, Y., Zhou, H., Zhen, X., et al. (2019). Transplantation of human endometrial perivascular cells with elevated CYR61 expression induces angiogenesis and promotes repair of a full-thickness uterine injury in rat. Stem Cell Res. Ther. *10*, 179.

22. Cao, Y., Sun, H., Zhu, H., Zhu, X., Tang, X., Yan, G., Wang, J., Bai, D., Wang, J., Wang, L., et al. (2018). Allogeneic cell therapy using umbilical cord MSCs on collagen scaffolds for patients with recurrent uterine adhesion: a phase I clinical trial. Stem Cell Res. Ther. *9*, 192.

23. Santamaria, X., Cabanillas, S., Cervelló, I., Arbona, C., Raga, F., Ferro, J., Palmero, J., Remohí, J., Pellicer, A., and Simón, C. (2016). Autologous cell therapy with CD133+ bone marrow-derived stem cells for refractory Asherman's syndrome and endometrial atrophy: a pilot cohort study. Hum. Reprod. *31*, 1087–1096.

24. March, C.M. (2011). Management of Asherman's syndrome. Reprod. Biomed. Online *23*, 63–76.

25. Yasmin, H., and Adeghe, J.H. (2004). Severe early-onset intrauterine growth restriction (IUGR) in a woman with Asherman's syndrome. J. Obstet. Gynaecol. *24*, 312–314.

26. Fukui, Y., Hirota, Y., Matsuo, M., Gebril, M., Akaeda, S., Hiraoka, T., and Osuga, Y. (2019). Uterine receptivity, embryo attachment, and embryo invasion: Multistep processes in embryo implantation. Reprod. Med. Biol. *18*, 234–240.

27. Fukuhara, S., Sako, K., Noda, K., Zhang, J., Minami, M., and Mochizuki, N. (2010). Angiopoietin-1/Tie2 receptor signaling in vascular quiescence and angiogenesis. Histol. Histopathol. *25*, 387–396.

28. Cervello, I., Gil-Sanchis, C., Santamaria, X., Cabanillas, S., Diaz, A., Faus, A., Pellicer, A., and Simon, C. (2015). Human CD133(+) bone marrow-derived stem cells promote endometrial proliferation in a murine model of Asherman syndrome. Fertility and Sterility *104*, 1552–1560.

29. Singh, N., Mohanty, S., Seth, T., Shankar, M., Bhaskaran, S., and Dharmendra, S. (2014). Autologous stem cell transplantation in refractory Asherman's syndrome: A novel cell based therapy. J. Hum. Reprod. Sci. *7*, 93–98.

30. Tan, J., Li, P., Wang, Q., Li, Y., Li, X., Zhao, D., Xu, X., and Kong, L. (2016). Autologous menstrual blood-derived stromal cells transplantation for severe Asherman's syndrome. Hum. Reprod. *31*, 2723–2729.

31. Nagori, C.B., Panchal, S.Y., and Patel, H. (2011). Endometrial regeneration using autologous adult stem cells followed by conception by in vitro fertilization in a patient of severe Asherman's syndrome. J. Hum. Reprod. Sci. *4*, 43–48.

32. Alawadhi, F., Du, H., Cakmak, H., and Taylor, H.S. (2014). Bone Marrow-Derived Stem Cell (BMDSC) transplantation improves fertility in a murine model of Asherman's syndrome. PLoS ONE *9*, e96662.

33. Kilic, S., Yuksel, B., Pinarli, F., Albayrak, A., Boztok, B., and Delibasi, T. (2014). Effect of stem cell application on Asherman syndrome, an experimental rat model. J. Assist. Reprod. Genet. *31*, 975–982.

34. Jing, Z., Qiong, Z., Yonggang, W., and Yanping, L. (2014). Rat bone marrow mesenchymal stem cells improve regeneration of thin endometrium in rat. Fertil. Steril. *101*, 587–594.

35. Zhao, J., Zhang, Q., Wang, Y., and Li, Y. (2015). Uterine infusion with bone marrow mesenchymal stem cells improves endometrium thickness in a rat model of thin endometrium. Reprod. Sci. *22*, 181–188.

36. Hu, J., Zeng, B., Jiang, X., Hu, L., Meng, Y., Zhu, Y., and Mao, M. (2015). The expression of marker for endometrial stem cell and fibrosis was increased in intrauterine adhesious. Int. J. Clin. Exp. Pathol. *8*, 1525–1534.

37. Wilcox, A.J., Baird, D.D., and Weinberg, C.R. (1999). Time of implantation of the conceptus and loss of pregnancy. N. Engl. J. Med. *340*, 1796–1799.

38. Song, H., Lim, H., Paria, B.C., Matsumoto, H., Swift, L.L., Morrow, J., Bonventre, J.V., and Dey, S.K. (2002). Cytosolic phospholipase A2alpha is crucial [correction of A2alpha deficiency is crucial] for 'on-time' embryo implantation that directs subsequent development. Development *129*, 2879–2889.

39. Baradwan, S., Baradwan, A., Bashir, M., and Al-Jaroudi, D. (2018). The birth weight in pregnant women with Asherman syndrome compared to normal intrauterine cavity: A case-control study. Medicine (Baltimore) *97*, e11797.

40. Ahmed, A., and Perkins, J. (2000). Angiogenesis and intrauterine growth restriction. Best Pract. Res. Clin. Obstet. Gynaecol. *14*, 981–998.

41. Sherer, D.M., and Abulafia, O. (2001). Angiogenesis during implantation, and placental and early embryonic development. Placenta *22*, 1–13.

42. Maybin, J.A., Murray, A.A., Saunders, P.T.K., Hirani, N., Carmeliet, P., and Critchley, H.O.D. (2018). Hypoxia and hypoxia inducible factor-1α are required for normal endometrial repair during menstruation. Nat. Commun. *9*, 295.

43. Plaisier, M., Dennert, I., Rost, E., Koolwijk, P., van Hinsbergh, V.W., and Helmerhorst, F.M. (2009). Decidual vascularization and the expression of angiogenic growth factors and proteases in first trimester spontaneous abortions. Hum. Reprod. *24*, 185–197.

44. Jun, S.M., Park, M., Lee, J.Y., Jung, S., Lee, J.E., Shim, S.H., Song, H., and Lee, D.R. (2019). Single cell-derived clonally expanded mesenchymal progenitor cells from somatic cell nuclear transfer-derived pluripotent stem cells ameliorate the endometrial function in the uterus of a murine model with Asherman's syndrome. Cell Prolif. *52*, e12597.

45. Lan, Y.W., Choo, K.B., Chen, C.M., Hung, T.H., Chen, Y.B., Hsieh, C.H., Kuo, H.P., and Chong, K.Y. (2015). Hypoxia-preconditioned mesenchymal stem cells attenuate bleomycin-induced pulmonary fibrosis. Stem Cell Res. Ther. *6*, 97.

46. Liu, Y., Tal, R., Pluchino, N., Mamillapalli, R., and Taylor, H.S. (2018). Systemic administration of bone marrow-derived cells leads to better uterine engraftment than use of uterine-derived cells or local injection. J. Cell. Mol. Med. *22*, 67–76.

47. Ebrahim, N., Mostafa, O., El Dosoky, R.E., Ahmed, I.A., Saad, A.S., Mostafa, A., Sabry, D., Ibrahim, K.A., and Farid, A.S. (2018). Human mesenchymal stem cell-derived extracellular vesicles/estrogen combined therapy safely ameliorates experimentally induced intrauterine adhesions in a female rat model. Stem Cell Res. Ther. *9*, 175.

48. Liu, F., Hu, S., Wang, S., and Cheng, K. (2019). Cell and biomaterial-based approaches to uterus regeneration. Regen. Biomater. *6*, 141–148.

49. Liu, F., Hu, S., Yang, H., Li, Z., Huang, K., Su, T., Wang, S., and Cheng, K. (2019). Hyaluronic Acid Hydrogel Integrated with Mesenchymal Stem Cell-Secretome to Treat Endometrial Injury in a Rat Model of Asherman's Syndrome. Adv. Healthc. Mater. *8*, e1900411.

50. Park, S.R., Kim, J.W., Jun, H.S., Roh, J.Y., Lee, H.Y., and Hong, I.S. (2018). Stem Cell Secretome and Its Effect on Cellular Mechanisms Relevant to Wound Healing. Mol. Ther. *26*, 606–617.

51. Yao, Y., Chen, R., Wang, G., Zhang, Y., and Liu, F. (2019). Exosomes derived from mesenchymal stem cells reverse EMT via TGF-β1/Smad pathway and promote repair of damaged endometrium. Stem Cell Res. Ther. *10*, 225.

52. Kawai, T., Katagiri, W., Osugi, M., Sugimura, Y., Hibi, H., and Ueda, M. (2015). Secretomes from bone marrow-derived mesenchymal stromal cells enhance periodontal tissue regeneration. Cytotherapy *17*, 369–381.

53. Dawar, F.U., Xiong, Y., Khattak, M.N.K., Li, J., Lin, L., and Mei, J. (2017). Potential role of cyclophilin A in regulating cytokine secretion. J. Leukoc. Biol. *102*, 989–992.

54. Jin, Z.G., Melaragno, M.G., Liao, D.F., Yan, C., Haendeler, J., Suh, Y.A., Lambeth, J.D., and Berk, B.C. (2000). Cyclophilin A is a secreted growth factor induced by oxidative stress. Circ. Res. *87*, 789–796.

55. Xue, C., Sowden, M.P., and Berk, B.C. (2018). Extracellular and Intracellular Cyclophilin A, Native and Post-Translationally Modified, Show Diverse and Specific Pathological Roles in Diseases. Arterioscler. Thromb. Vasc. Biol. *38*, 986–993.

56. Kalinina, A., Zamkova, M., Antoshina, E., Trukhanova, L., Gorkova, T., Kazansky, D., and Khromykh, L. (2019). Analyses of the toxic properties of recombinant human Cyclophilin A in mice. J. Immunotoxicol. *16*, 182–190.

57. Satoh, K. (2015). Cyclophilin A in cardiovascular homeostasis and diseases. Tohoku J. Exp. Med. *235*, 1–15.

58. Satoh, K., Matoba, T., Suzuki, J., O'Dell, M.R., Nigro, P., Cui, Z., Mohan, A., Pan, S., Li, L., Jin, Z.G., et al. (2008). Cyclophilin A mediates vascular remodeling by promoting inflammation and vascular smooth muscle cell proliferation. Circulation *117*, 3088–3098.

59. Zhang, H., Chen, J., Liu, F., Gao, C., Wang, X., Zhao, T., Liu, J., Gao, S., Zhao, X., Ren, H., and Hao, J. (2014). CypA, a gene downstream of HIF-1α, promotes the development of PDAC. PLoS ONE *9*, e92824.

60. Han, H.J., Kwon, N., Choi, M.A., Jung, K.O., Piao, J.Y., Ngo, H.K., Kim, S.J., Kim, D.H., Chung, J.K., Cha, Y.N., et al. (2016). Peptidyl Prolyl Isomerase PIN1 Directly Binds to and Stabilizes Hypoxia-Inducible Factor-1α. PLoS ONE *11*, e0147038.

61. Perrucci, G.L., Straino, S., Corlianò, M., Scopece, A., Napolitano, M., Berk, B.C., Lombardi, F., Pompilio, G., Capogrossi, M.C., and Nigro, P. (2016). Cyclophilin A modulates bone marrow-derived CD117(+) cells and enhances ischemia-induced angiogenesis via the SDF-1/CXCR4 axis. Int. J. Cardiol. *212*, 324–335.

62. An, B., Na, S., Lee, S., Kim, W.J., Yang, S.R., Woo, H.M., Kook, S., Hong, Y., Song, H., and Hong, S.H. (2015). Non-enzymatic isolation followed by supplementation of basic fibroblast growth factor improves proliferation, clonogenic capacity and SSEA-4 expression of perivascular cells from human umbilical cord. Cell Tissue Res. *359*, 767–777.

63. Cho, A., Park, S.R., Kim, S.R., Nam, S., Lim, S., Park, C.H., Lee, H.Y., and Hong, I.S. (2019). An Endogenous Anti-aging Factor, Sonic hedgehog, Suppresses Endometrial Stem Cell Aging through SERPINB2. Molecular therapy, 1286–1298.

64. Yoon, B.S., Moon, J.H., Jun, E.K., Kim, J., Maeng, I., Kim, J.S., Lee, J.H., Baik, C.S., Kim, A., Cho, K.S., et al. (2010). Secretory profiles and wound healing effects of human amniotic fluid-derived mesenchymal stem cells. Stem cells and development, 887–902.

65. Rutledge, R.G., and Côté, C. (2003). Mathematics of quantitative kinetic PCR and the application of standard curves. Nucleic Acids Res. *31*, e93.

66. Kim, H.R., Kim, Y.S., Yoon, J.A., Lyu, S.W., Shin, H., Lim, H.J., Hong, S.H., Lee, D.R., and Song, H. (2014). Egr1 is rapidly and transiently induced by estrogen and bisphenol A via activation of nuclear estrogen receptor-dependent ERK1/2 pathway in the uterus. Reprod. Toxicol. *50*, 60–67.

YMTHE, Volume *28*

Supplemental Information

Perivascular Stem Cell-Derived Cyclophilin A Improves Uterine Environment with Asherman's Syndrome via HIF1α-Dependent Angiogenesis

Mira Park, Seok-Ho Hong, So Hee Park, Yeon Sun Kim, Seung Chel Yang, Hye-Ryun Kim, Songmi Noh, Sunghun Na, Hyung Keun Lee, Hyunjung J. Lim, Sang Woo Lyu, and Haengseok Song

Figure S1

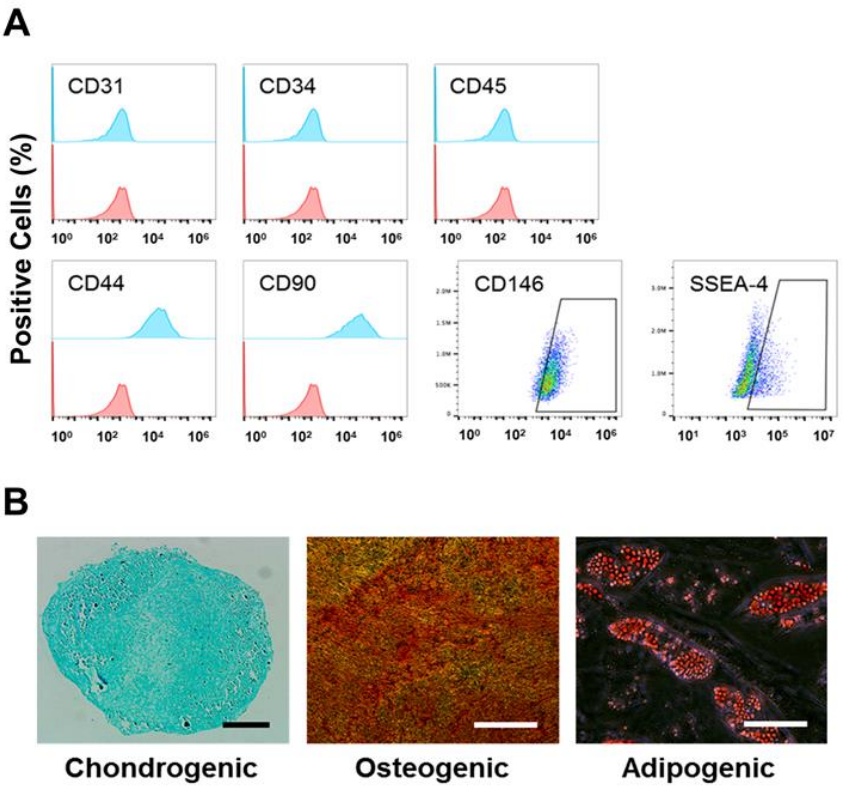

Figure S1. Molecular and cellular characterization of hPVSCs as MSCs. (A) Representative flow cytometry histograms and dot plots for phenotypic analyses of hPVSCs (passage 2). The pink histograms show the isotype control. (B) Multilineage differentiation of hPVSCs. Representative images of Alcian blue staining of chondrocytes, Alizarin Red S staining of osteocytes, and Oil Red O staining of adipocytes. Scale bar: 100 μm.

Figure S2

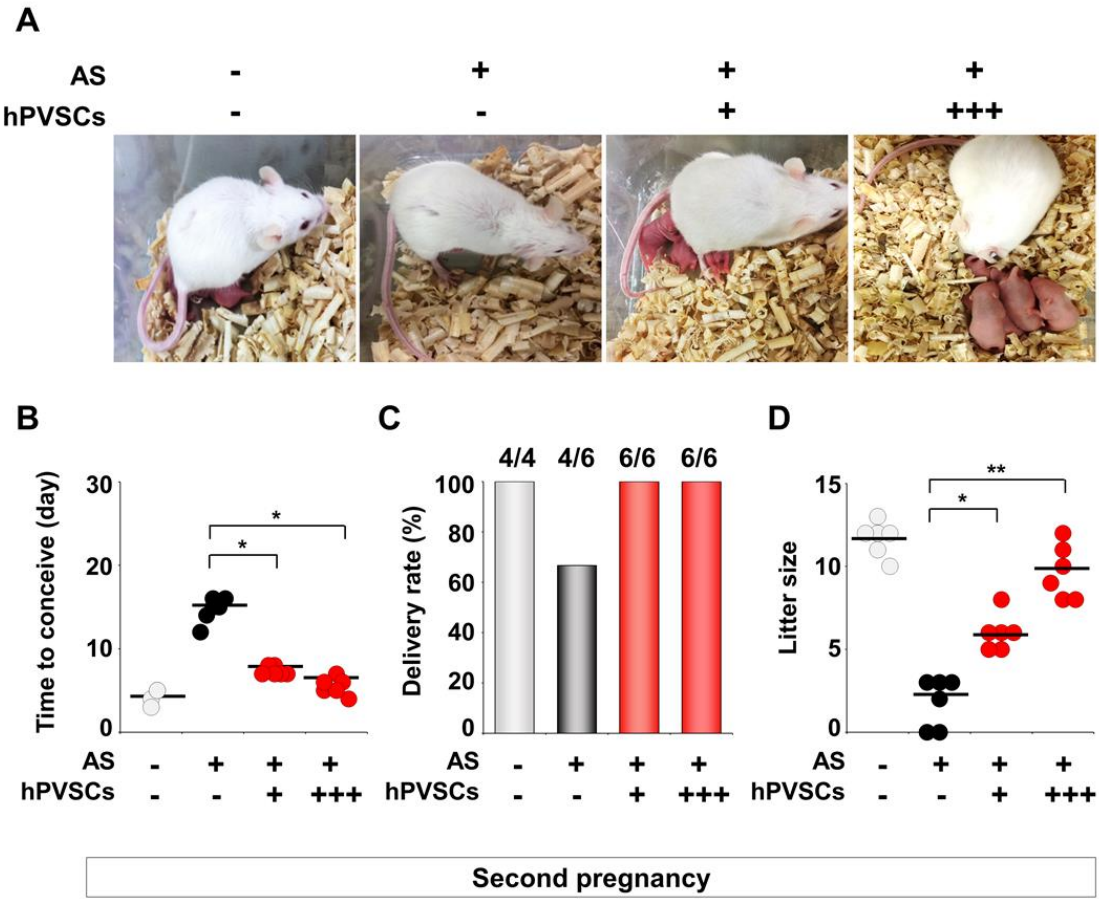

Figure S2. Therapeutic actions of hPVSCs on chronic reproductive impairments in mice with AS. (A) Representative photographs of mice with AS after the second delivery. +; IU delivery of hPVSCs (1×10^6), +++; a single IU followed by 3 IP delivery of hPVSCs (1×10^6). Therapeutic effects of hPVSCs on time to conceive (B), delivery rate (C), and litter size (D) in the second pregnancies of mice with AS. The horizontal black lines represent median values. Numbers above the bars indicate the number of mice that delivered live pup(s)/total mice examined. *; $P<0.05$, **; $P<0.01$.

Figure S3

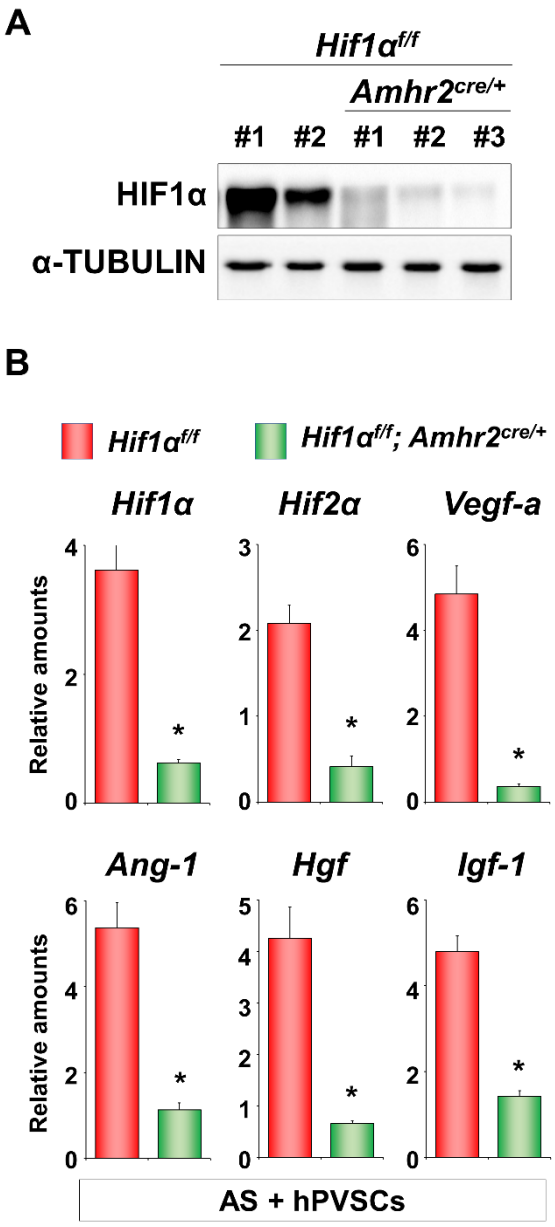

Figure S3. Conditional deletion of uterine Hif1α using AmhR2-Cre and expression of angiogenic factors in *Hif1α$^{f/f}$;Amhr2$^{cre/+}$* mice with AS after hPVSCs therapy. (A) Western blotting for the HIF1α deletion in the uteri of *Hif1α$^{f/f}$; Amhr2$^{cre/+}$* mice. α-TUBULIN was used as the loading control. (B) Real-time RT-PCR analyses of expression of angiogenesis-related factors in *Hif1α$^{f/f}$;Amhr2$^{cre/+}$* mice with AS after hPVSCs transplantation.

Figure S4

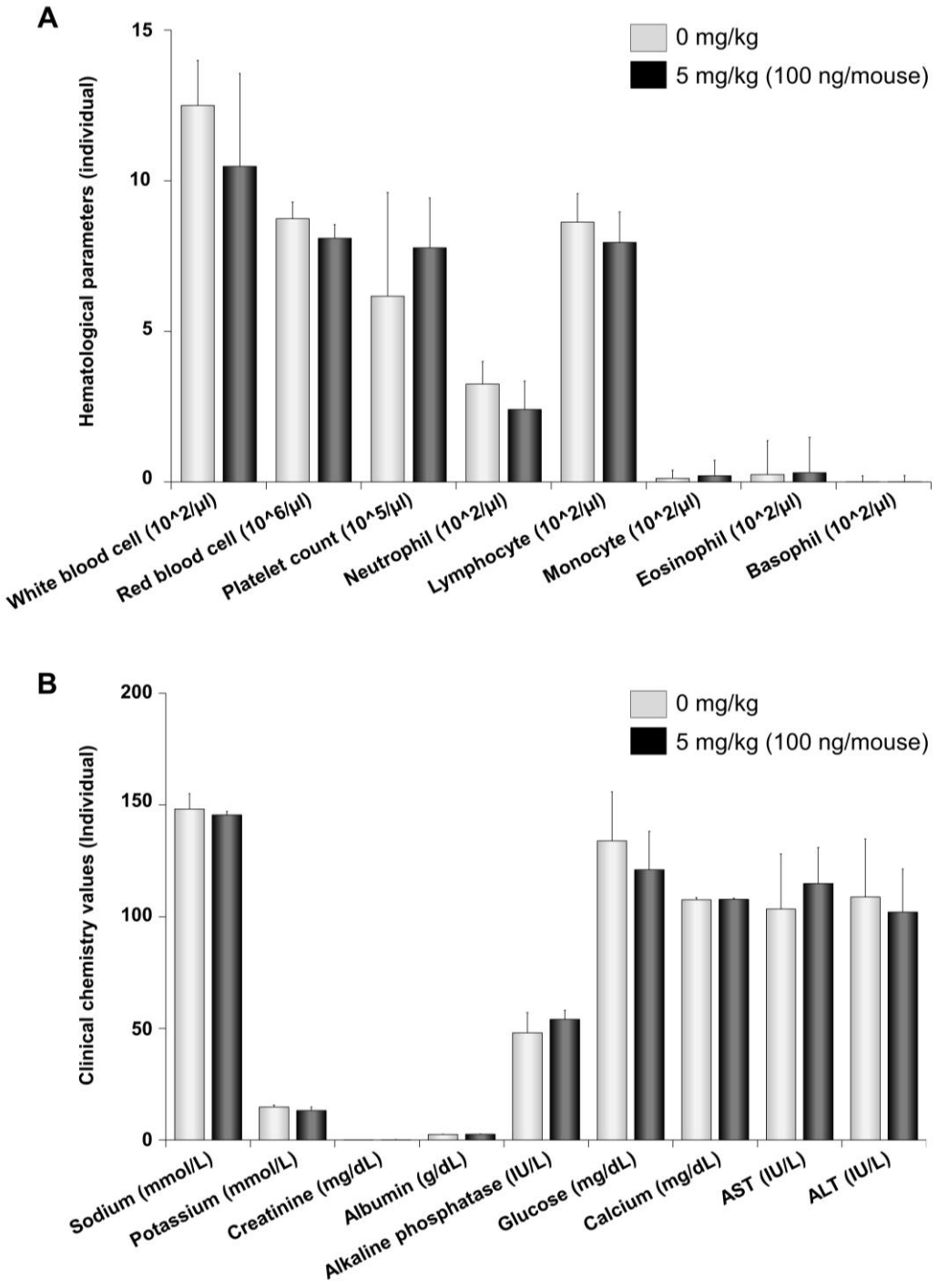

Figure S4. Immune cell profiles and general toxicity in mice after intrauterine administration of CYP-A at 100 ng/mouse. Cell count analyses of various immune cells of whole blood (A) and biochemical assays of serum (B) 24 h after CYP-A treatment. AST; aspartate transaminase, ALT; alanine transaminase.

Table S1. List of secreted proteins from human perivascular stem cells

No.	Protein name	NCBI BLAST	Score	Mass
1	Profilin-1	NP_005013.1	1071	15225
	Cystatin-C precursor	NP_000090.1	70	16029
2	Peptidylprolyl isomerase A (Cyclophilin A)	AAH07104.1	1025	18239
	hCG2016877, isoform CRA_c	EAW74247.1	81	44298
	Transgelin	NP_003177.2	73	22674
	Hypothetical protein, partial	CAH18175.1	46	199821
	Collagen, type V, alpha 2, isoform CRA_b	EAX10907.1	41	86488
	Collagen alpha-2(V) chain	CAA28454.1	41	106111
	Mucin short variant	AAK30142.1	40	18378
3	Tropomyosin beta chain isoform Tpm2.1sm/cy	NP_998839.1	389	33050
4	Cofilin-1	NP_005498.1	182	18724
	Cofilin-2 isoform 1	NP_068733.1	60	18848
	PEX5-related protein isoform X8	XP_011511190.1	41	66711
5	Crystal Structure of Anthrax Edema Factor	1XFU_O	126	16839
	Macrophage expressed 1	AAI12231.1	42	79660
6	Cadherin 2, type 1, N-cadherin (neuronal)	EAX01239.1	113	94379
	Keratin 13 (KRT13), transcript variant 1	BAF82933.1	67	49869
7	Transgelin variant, partial	BAD92792.1	68	12321
	UTP15 protein	AAH13064.1	47	32546
	Apolipoprotein B mRNA editing enzyme	BAD92216.1	46	25657
	cDNA FLJ13705 fis, clone PLACE2000302	BAB14672.1	40	23050
8	Plasminogen	AAH60513.1	47	93333
9	Coiled-coil domain-containing protein 180	Q9P1Z9.2	43	192570
	Actin-related protein 2/3 complex	NP_005708.1	41	16381

Table S2. Primer sequences for genotyping

Genotype		Sequence (5'-3')	Size (bp)
Hif1α$^{f/f}$	Forward	TGCATGTGTATGGGTGTTTTG	WT: 99
	Reverse	GAAAACTGTCTGTAACTTCATTTCC	f/f: 120
Amhr2$^{cre/+}$	Forward	GGACATGTTCAGGGATCGCCAGGC	Cre: 219
	Reverse	CGACGATGAAGCATGTTTAGCTG	

Table S3. Primer sequences for RT-PCR and real-time RT-PCR

Gene		Sequence (5'-3')	Size (bp)
Col1a1	Forward	CTGGCGGTTCAGGTCCAAT	141
	Reverse	TTCCAGGCAATCCACGAGC	
Timp1	Forward	GGGTTCCCCAGAAATCAACGAG	139
	Reverse	ACAGAGGCTTTCCATGACTGGGGTG	
Tgfβ1	Forward	GTGAAACGGAAGCGCATCGAAG	193
	Reverse	CATAGTAGTCCGCTTCGGGCTCC	
Tnfα	Forward	CTGAACTTCGGGGTGATCGG	122
	Reverse	GGCTTGTCACTCGAATTTTGAGA	
Hif1α	Forward	ACAAGTCACCACAGGACAG	168
	Reverse	AGGGAGAAAATCAAGTCG	
Hif2α	Forward	AATGACAGCTGACAAGGAGAAAAA	257
	Reverse	GAGTGAAGTCAAAGATGCTGTGTC	
Vegf-a	Forward	GCAGGCTGCTGTAACGATGA	105
	Reverse	GCATGATCTGCATGGTGATGTT	
Ang-1	Forward	GGGACAGCAGGCAAACAGA	110
	Reverse	TGTCGTTATCAGCATCCTTCGT	
Hgf	Forward	CTGACCCAAACATCCGAGTTG	125
	Reverse	TTCCCATTGCCACGATAACAA	
Igf-1	Forward	TGCTTCCGGAGCTGTGATCT	125
	Reverse	CGGGCTGCTTTTGTAGGCT	